External synchronization of oscillating pulse edge on a transmission line with regularly spaced tunnel diodes

Koichi Narahara*
Graduate School of Science and Engineering, Yamagata University, 4-3-16 Jonan, Yonezawa, Yamagata 992-8510, Japan

Masatoshi Misono and Kenji Miyakawa
Department of Applied Physics, Faculty of Science, Fukuoka University, 8-19-1 Nanakuma, Jonan, Fukuoka, Fukuoka 814-0180, Japan
(Received 30 September 2012; published 3 January 2013)

We investigate the external synchronization of the oscillating pulse edges developed in a transmission line periodically loaded with tunnel diodes (TDs), termed a TD line. It is observed that the pulse edge oscillates on a TD line when supplied by an appropriate voltage at the end of the line. We discuss how the pulse edge oscillates on a TD line and the properties of the external synchronization of the edge oscillation driven by a sinusoidal perturbation. By applying a phase-reduction scheme to the transmission equation of a TD line, we obtain the phase sensitivity, which satisfactory explains the measured spatial dependence of the locking range on the frequency. Moreover, we successfully detect the spatiotemporal behaviors of the edge oscillation by establishing synchronization with the sampling trigger of an oscilloscope.

DOI: 10.1103/PhysRevE.87.012902 PACS number(s): 05.45.Xt, 41.20.−q, 85.30.Mn

I. INTRODUCTION

The nonlinear wave properties in a transmission line that is periodically loaded with tunnel diodes (TDs), referred to as a TD line for brevity, have attracted attention in the fields of both science and engineering. Because the TD line adequately simulates the nerve axon on the basis of the Hodgkin-Huxley model, it is used in the field of physiology to characterize the electrical pulses propagating on a nerve axon [1]. By arranging the unit-cell structure, the nonattenuating propagation of electrical pulses on a nerve axon is appropriately demonstrated. Nagumo *et al.* [2] considered a TD line whose unit cell consists of a shunt TD, a series resistor, and a shunt inductor that feeds the appropriate dc voltage. They found that only a voltage pulse having an amplitude higher than a certain threshold could propagate on the line and evolve into a pulse with an inherent waveform. These properties qualitatively explain the actual behavior of an electrical pulse on a nerve axon. Richer [3] considered the propagation of a voltage edge on a TD line consisting of a series resistor and a shunt TD in each unit cell. It was observed that the edge became stable, i.e., it evolved into a traveling front that preserved the shape and velocity and could propagate on the line only in a specific direction, such that the voltage level decreased at every cell through which the edge passed.

On the other hand, the use of a TD line has been investigated in high-speed electronics. For use at high frequencies, each TD is connected by a series inductor. By setting the appropriate biasing voltage and current for the line, a steep incident pulse edge is generated by the loaded TDs [4]. A resonant tunneling diode (RTD), which is fabricated using compound semiconductor materials, is widely used. Oscillators using a state-of-the-art RTD generate submillimeter and terahertz waves at room temperature [5]. Moreover, RTDs are employed on a TD line to generate a broadband voltage front up to millimeter wave frequencies [6–8]. In addition, several schemes using TD lines have been reported to date for generating short electrical pulses [9,10]. Recently, an interesting oscillation was observed for a voltage edge on a TD line [11]. With an appropriate boundary condition, a voltage edge repeatedly turned around halfway on the line.

In this paper, we investigate the external synchronization of the oscillating pulse edges in a TD line. External synchronization is the most fundamental synchronization phenomenon observed in a limit cycle [12] that is one-sidedly affected by an external oscillation. Most of the familiar examples include the circadian rhythms. If the nature of an external oscillation including the amplitude, phase, and waveform is known *a priori*, the properties of a limit cycle can be clarified through external synchronization. We find that the edge oscillation in a TD line is a kind of limit cycle and can be synchronized with a known sinusoidal perturbation.

Because the edge oscillation develops on a spatially extended platform, the locking range may depend on the cell to which the external oscillation is assigned. To quantify the locking efficiency, we apply a phase-reduction scheme [13] to the transmission equations of a TD line. The identity of a limit cycle is illustrated by the phase sensitivity, which quantifies how the phase of the limit cycle responds to perturbation. To obtain a consistent spatial dependence on frequency considering the measured locking range, we employ the standard numerical procedure to calculate the phase sensitivity. The qualitative validity of the phase sensitivity is successfully confirmed in a spatially extended limit cycle.

In addition to the fundamental edge oscillation, we detect another oscillation mode only through measurements. This secondary (s) mode requires two oscillating edges that originate at a cell halfway along the TD line. These edges are mutually synchronized to support a stable oscillation. Moreover, the turnaround distance of the edge in the s mode is approximately half that in the fundamental (f) mode; therefore, the second-harmonic component of the f mode excites the s mode. These properties are directly observed in measurements.

*narahara@yz.yamagata-u.ac.jp

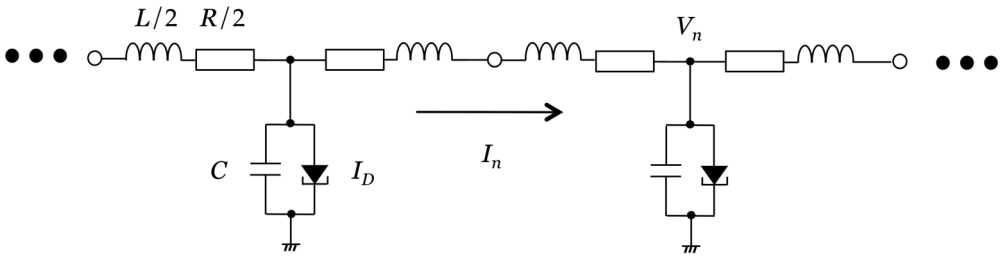

FIG. 1. Cell structure of TD lines. Two adjacent cells are shown. The line inductance, resistance, capacitance, and diode current are represented by L, R, C, and I_D, respectively.

In Sec. II, we discuss the structure and fundamental properties of a traveling front or shock wave and edge oscillation in a TD line. In Sec. III, we discuss the numerical evaluation of the external synchronization observed in edge oscillations. The experimental characterization of edge oscillations is discussed in Sec. IV.

II. EDGE OSCILLATION IN TD LINES

Figure 1 shows the unit cell of a TD line, where L, R, C, and I_D represent the series inductance, series resistance, shunt capacitance, and current of the shunt TD of the unit cell, respectively. The typical current-voltage relationship of a TD is shown as the thick dashed curve in Fig. 2. There are two characteristic voltages, the peak and valley voltages, denoted V_p and V_v, respectively. TDs exhibit a negative differential resistance at voltages between V_p and V_v. In general, any type of TD, including Esaki diodes and RTDs, can be used as a platform to develop edge oscillation, which is under investigation.

Consider the case in which a DC voltage, whose value surpasses V_p, is applied to one of the ends of a TD line, whose cells are all initially set to zero. Then a voltage edge develops and starts propagating on the line. Let the line current flowing to the nth cell and the line voltage at the nth cell be I_n and V_n, respectively. Then the transmission line equations are given by

$$\frac{dI_n}{dt} = \frac{V_{n-1} - V_n - RI_n}{L}, \tag{1}$$

$$\frac{dV_n}{dt} = \frac{I_n - I_{n+1} - I_D(V_n)}{C}. \tag{2}$$

When the propagating voltage edge extends over many cells, we approximate the above equations using a continuous spatial variable x to obtain

$$LC\frac{\partial^2 V}{\partial t^2} + \left(CR + L\frac{dI_D(V)}{dV}\right)\frac{\partial V}{\partial t} = \frac{\partial^2 V}{\partial x^2} - RI_D(V), \tag{3}$$

where $V = V(x,t)$ represents the continuous counterpart of V_n. Moreover, L, C, R, and I_D are rescaled to be per-unit-length quantities. Equation (3) is a nonlinear hyperbolic equation and can support traveling fronts, i.e., uniformly translating solutions with constant speeds [14].

To investigate the dynamics of the voltage edge on a TD line, we use the method developed by Hadeler and Rothe in [15]. We model the diode current to exhibit the current-voltage relationship with $\beta_0 > 0$, as shown in

$$I_D(V) = \beta_0 V(V - V_{\rm th})(V - V_0), \tag{4}$$

where V represents the voltage across the terminals. The property of the test diode is shown by the solid curve in Fig. 2. Unlike TDs, the current disappears at three voltages, namely, 0, $V_{\rm th}$, and V_0.

We consider that the traveling fronts connecting the equilibrium voltages $V = V_{\rm th}$ and $V = 0$ have a velocity of c. By introducing the solution of the form $V(x - ct)$ to Eq. (3), we obtain the ordinary differential equation

$$(c^2LC - 1)V'' - c\left(CR + L\frac{dI_D(V)}{dV}\right)V' + RI_D(V) = 0, \tag{5}$$

where a prime denotes differentiation with respect to $\xi = x - ct$. By introducing the variables $u = V/V_{\rm th}$ and $v = u'$ and assuming that $c \neq 1/\sqrt{LC}$, Eq. (5) becomes a first-order system:

$$u' = f(u,v,c) = v, \tag{6}$$

$$v' = g(u,v,c) = \frac{1}{c^2LC - 1}\left\{cv\left(CR + L\frac{dI_D(V_{\rm th}u)}{dV}\right) - \frac{R}{V_{\rm th}}I_D(V_{\rm th}u)\right\}. \tag{7}$$

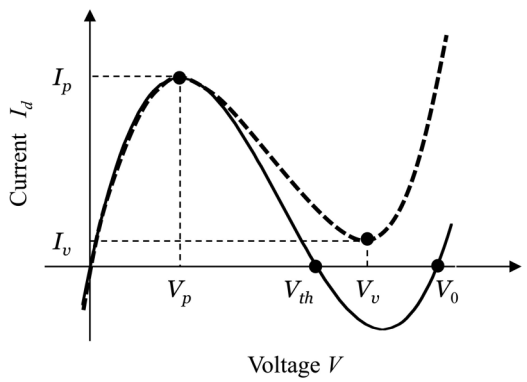

FIG. 2. Current-voltage relationship of TDs. The thick dashed curve represents the typical current-voltage relationship of a TD. The peak and valley voltages are represented by V_p and V_v, respectively. On the other hand, the solid curve shows the model function $I_D(V) \propto V(V - V_{\rm th})(V - V_0)$, where V is the voltage across terminals, which provides the fundamental properties of a TD line.

There are two singular points in $(u,v) \in [0,1] \times [0,\infty)$, namely, points $P_1(0,0)$ and $P_2(1,0)$, whose types are summarized as follows.

For $c < 1/\sqrt{LC}$, P_1 is a saddle point whose unstable directions satisfy $dv/du > 0$, whereas it is an unstable node for $c > 1/\sqrt{LC}$, whose main and side directions satisfy $dv/du < 0$. On the other hand, P_2 is a focus for $c < c_0$ defined as

$$c_0 = \frac{2\sqrt{R\,|G_1|}}{CR + L\,|G_1|}, \tag{8}$$

where $G_1 < 0$ represents the differential conductance at $V = V_{\rm th}$, i.e., $G_1 = dI_D(V_{\rm th})/dV$. The focus becomes stable for $CR + LG_1 < 0$ and unstable for $CR + LG_1 > 0$. For $c \in (c_0, 1/\sqrt{LC})$, P_2 is a stable node, whose main and side directions satisfy $dv/du < 0$. Moreover, P_2 is a saddle point for $c > 1/\sqrt{LC}$, whose unstable direction satisfies $dv/du < 0$.

When $CR + Ld I_D/dV > 0$ for all $u \in (0,1)$, the system satisfies all the assumptions required in Theorem 1 of [14] for $c \in (c_0, 1/\sqrt{LC})$; therefore, it is established that a unique traveling front is supported by a TD line. For greater c, a shock wave develops. In either case, the edge can stably propagate on a TD line. Refer to the Appendix for the detailed properties of traveling fronts and shock waves.

In practical situations, the line must have boundaries, where the voltage front (or shock wave) may be reflected and start propagating in the opposite direction. This reflected front must correspond to a trajectory in the phase plane that starts at P_2 and possibly reaches a certain point in the lower half-plane; therefore, the reflected edge can develop only for $c \in (0, c_0)$ and $CR + LG_1 > 0$, where P_2 becomes an unstable focus. Because a front propagating to P_2 develops robustly, the reflected edge is supposed to be replaced by such a front on the line. Certain transient processes cannot be described by Eqs. (6) and (7). However, the estimated behavior of the phase point is shown in Fig. 3 for qualitative illustration. Let the values of c for the traveling front and reflected wave be c_f and c_r, respectively. Then, at $c = c_r$ ($< c_0$), P_2 becomes an unstable focus. Then a reflected edge starts following the spiral trajectory and reaches point P_1 through the lower half-plane $v < 0$. Then a front starts at P_1 and propagates toward P_2, such that the trajectory reaches and returns from P_2 on the $c = c_f$ plane.

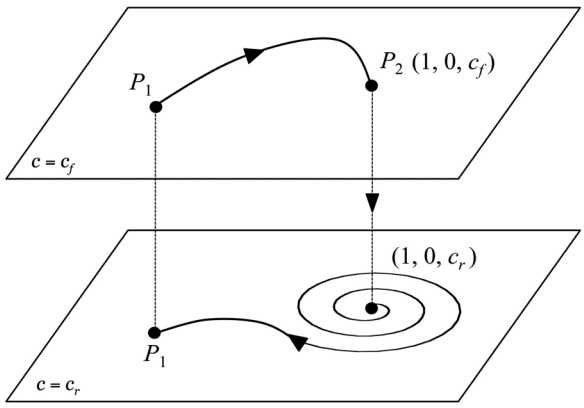

FIG. 3. Sample trajectory corresponding to edge oscillation. At $c = c_r$, point (1,0) becomes an unstable focus. On the other hand, it becomes a stable node for $c = c_f$.

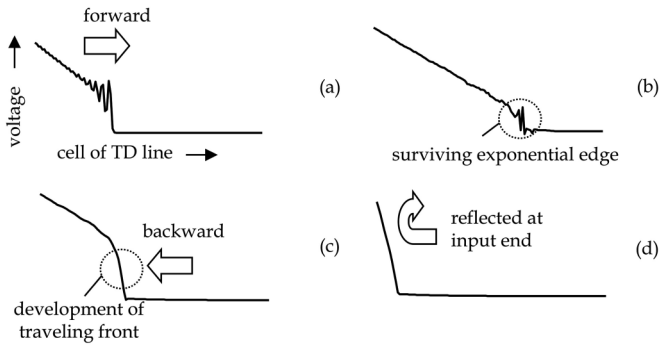

FIG. 4. Fundamental oscillation mode of the pulse edge in a TD line. Time progresses from (a) to (d). The reflected edge in (d) starts to travel forward again, resulting in edge oscillation. The horizontal axis measures the spatial dimension, which must be originally discrete.

Figure 4 illustrates the behavior of line voltage corresponding to the phase-plane trajectory in Fig. 3. The spatial position on the TD line is shown horizontally and the voltage is shown vertically. Point P_2 in Fig. 3 corresponds to the input end of a TD line that is biased to develop a voltage edge. Then Fig. 4(a) shows the behavior of line voltage corresponding to the phase-plane trajectory on the $c = c_r$ plane. The voltage edge that exhibits oscillation corresponds to the spiral part of the phase-plane trajectory. Because of the losses and leakage, the edge is gradually attenuated, and it nearly disappears, as shown in Fig. 4(b). At this stage, a stable traveling front develops and starts propagating back to P_2 as shown in Fig. 4(c). Once the voltage edge returns to the input end, it is reflected again to propagate from the input end as shown in Fig. 4(d). The voltage edge repeats this process to oscillate on the line. This is the f mode of oscillation. Moreover, we refer to the directions *from* and *to* the input end as the *forward* and *backward* directions, respectively.

If the input is connected to an ideal voltage source without internal resistance, the voltage of the input cell is fixed to a constant value and consequently the reflected edge is not influenced by the input boundary. Therefore, the reflected edge gradually becomes identical to the previously reflected edge. On the other hand, for practical voltage sources, the voltage at the input cell cannot recover its original value within the CR time constant provided by the source's internal resistance. The presence of two different time scales, including the turnaround time of the propagating edge and the CR time constant at the input boundary, can make the edge oscillation quasiperiodic. Through numerical evaluations, the velocity of the voltage edge does not significantly depend on the input dc voltage. Moreover, the edge propagates further, and the turnaround time increases for greater input dc voltage [16]. This is because the frequency of the edge oscillation decreases as the input dc voltage increases.

For actual TDs, a finite current flows, even at $V = V_v$ (I_v in Fig. 2), so that the traveling front cannot develop. However, edge oscillation requires only the transient development of fronts; therefore, it may be established in a practical TD line. In addition, this concept is predicted by the heuristic description based on the transmission-line theory [11], which provides some insight into the frequency of the oscillatory component of the reflected voltage edge.

III. EXTERNAL SYNCHRONIZATION IN TD LINES

After introducing several results of the time-domain calculations including the oscillation frequency and the spatial transient of an edge, we apply the phase-reduction scheme to edge oscillations in a TD line to examine the external synchronization of edge oscillations with a sinusoidal perturbation, which is used to evaluate the cell dependence of the phase sensitivity.

We consider an N-cell TD line. Initially, all line voltages are set to zero. Then the input end is connected to a voltage source with negligible internal resistance that outputs the dc voltage of A and the other end is short-circuited. For convenience, we define $2N$ variables X_i $(i = 1, \ldots, 2N)$ as $X_m = I_m$ and $X_{N+m} = V_m$ for $m = 1, \ldots, N$. Then Eqs. (1) and (2) can be reformulated as

$$\frac{d\mathbf{X}}{dt} = \mathbf{F}(\mathbf{X}), \tag{9}$$

where $\mathbf{X} = (X_1, \ldots, X_{2N})$ and $\mathbf{F}$ represents a $2N$ vector defined by

$$\begin{aligned} F_1 &= \frac{1}{L}\left(A - X_{N+1} - RI_1\right), \\ F_i &= \frac{1}{L}\left(X_{N+i-1} - X_{N+i} - RI_i\right), \end{aligned} \tag{10}$$

$$F_{N+j} = \frac{1}{C}(X_j - X_{j+1} - I_D(X_{N+j})),$$

$$F_{2N} = \frac{1}{C}(X_N - I_D(X_{2N})) \tag{11}$$

for $i = 2, \ldots, N$ and $j = 1, \ldots, N-1$. F_1 and F_{2N} account for the boundary conditions. The fourth-order Runge-Kutta method was used to solve Eq. (9). In order to simulate the measured TD line discussed below, we set L, C, and R to 1.0 μH, 500.0 pF, and 1.0 Ω, respectively. I_D was optimized to exhibit the relationship shown by the thick dashed line in Fig. 2, where V_p, V_v, I_p, and I_v were set to 60.0 mV, 380.0 mV, 6.0 mA, and 1.1 mA, respectively. After an appropriate calculation time had elapsed, the voltage edge started oscillating steadily. We examined this steady state.

The spatiotemporal waveform for $A = 0.7$ V is shown in Fig. 5. The brighter points exhibit higher line voltages. A single voltage edge develops and oscillates. Therefore, it is confirmed that edge oscillation is supported by the f mode for all of the calculated input dc voltages. Spatial waveforms are shown in Figs. 6(a), 6(b), 6(c), and 6(d), which correspond to the timings of 0.5, 0.7, 0.8, and 1.15 μs in Fig. 5, respectively. When a stable front develops as shown in Fig. 6(b), the voltage edge starts propagating backward as shown in Fig. 6(c). Once the edge returns to the input end, it is again reflected to propagate forward as shown in Fig. 6(d). The edge that is propagating forward exhibits an oscillatory behavior as shown in Fig. 6(a), whereas the backward edge does not, as shown in Fig. 6(c). These results are the same as those observed in Fig. 4. At a fixed cell, the voltage rapidly decreases to zero when the backward edge passes it, and the voltage rapidly attains a certain finite value when the forward edge passes the cell. Therefore, the temporal waveform monitored at the point is a train of square pulses, whose fundamental frequency is coincident with that of the edge oscillation. Therefore, the spectral peaks

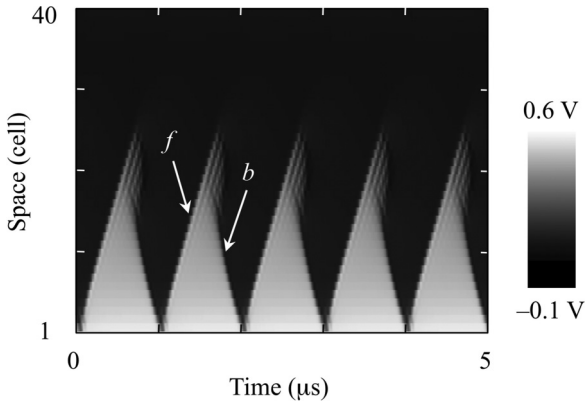

FIG. 5. Spatiotemporal behaviors of the calculated f-mode waveforms for $A = 0.7$ V. Brighter points exhibit higher line voltages. Forward- and backward-going edges are designated f and b, respectively.

corresponding to the fundamental and high-order harmonics may be observed in the spectrum. We monitored the fifth cell, where the duty cycle of the pulse train is moderate for all of the input dc voltages.

Figure 7(a) shows the spectral peaks calculated by the Fourier transforms of the temporal waveforms monitored at the fifth cell for different input dc voltages. The horizontal and vertical axes measure the input dc voltage and frequency, respectively. The four sequences of spectral peaks are observed in Fig. 7(a), each corresponding to the harmonics up to the fourth order. For $A < 0.6$ V, the oscillation frequency decreases as A increases, depending on the turnaround time. On the other hand, the oscillation frequency does not significantly depend on A for values above 0.6 V, being sufficiently greater than V_v, because a considerable increase in I_D protects the frequency from the impact of the increasing dc voltage.

In order to model an external perturbation, the transmission equation is modified by a $2N$ vector $\mathbf{p}(t)$ with $\epsilon \ll 1$ as

$$\frac{d\mathbf{X}}{dt} = \mathbf{F}(\mathbf{X}) + \epsilon\mathbf{p}(t). \tag{12}$$

We investigated the situation in which only the Mth cell was externally perturbed by a sinusoidal voltage with an angular frequency of ω_1. Then the components of $\mathbf{p}$ are given as $p_{N+M} = \sin(\omega_1 t)$ and $p_i = 0$ for the other values of i. According to the phase-reduction scheme [13], by defining the phase ϕ of the limit cycle for the angular frequency to be ω, the temporal evolution of the phase difference between the limit cycle and the sinusoidal perturbation $\psi = \phi - \omega_1 t$ is given by [13]

$$\frac{d\psi}{dt} = \Delta\omega + \Gamma(\psi), \tag{13}$$

$$\Gamma(\psi) = \frac{1}{2\pi}\int_0^{2\pi} d\theta\, \mathbf{Z}(\theta + \psi)^T \mathbf{q}(\theta), \tag{14}$$

where $\Delta\omega = \omega - \omega_1$ and $\mathbf{q}(\omega_1 t) = \mathbf{p}(t)$. The identity of the edge oscillation is represented by the 2π-periodic $2N$-vector function $\mathbf{Z}(\phi) = \nabla_{\mathbf{X}}\phi$, which is called the phase sensitivity. When the right-hand side of Eq. (13) becomes zero for a certain ψ and $d^2\psi/dt^2 < 0$, ψ becomes time invariant for a sufficiently large period of time. Therefore, the edge oscillation

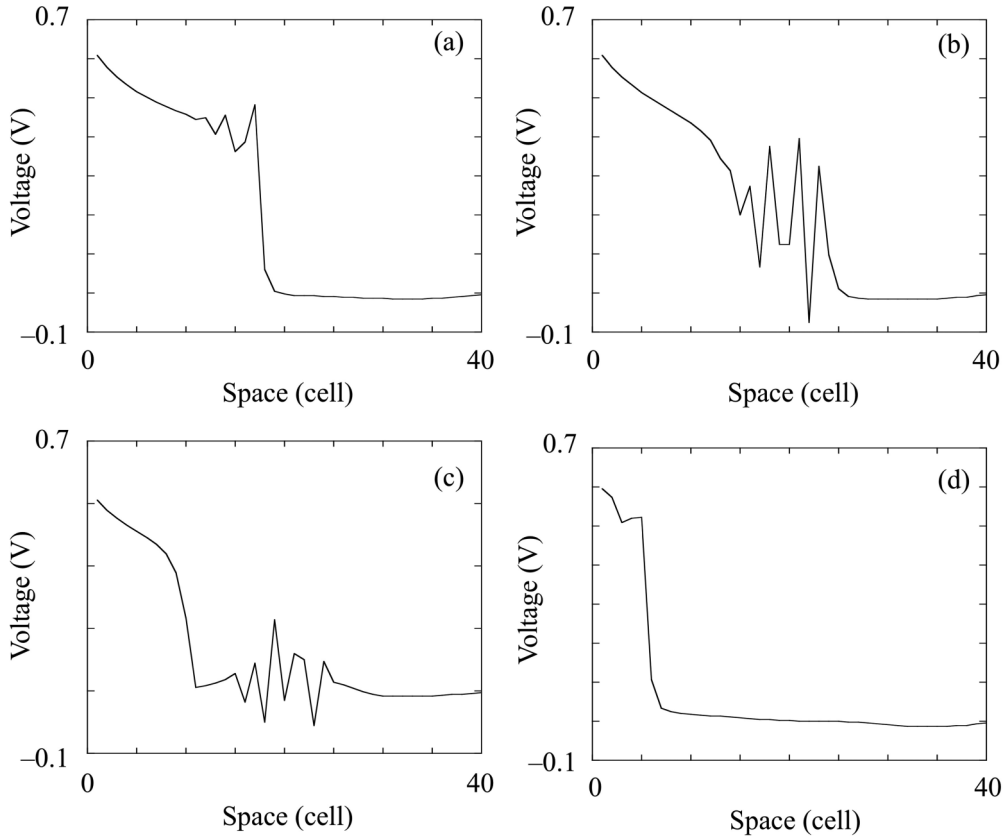

FIG. 6. Four temporal slices in Fig. 5 at the timings of (a) 0.5 μs, (b) 0.7 μs, (c) 0.8 μs, and (d) 1.15 μs.

is phase locked with the sinusoidal perturbation. Hence, when the variation of $\Gamma(\psi)$ with respect to ψ increases, the locking frequency range $\Delta\omega$ also increases. Thus, for measuring the efficiency of external synchronization, we consider the quantity defined by

$$\Delta\Gamma = \left| \max_{0<\psi\leqslant 2\pi} \Gamma(\psi) - \min_{0<\psi\leqslant 2\pi} \Gamma(\psi) \right|. \qquad (15)$$

The phase sensitivity is numerically obtained by solving the adjoint of the linearized Eq. (9) with the initial condition that the eigenvector corresponds to the eigenvalue 1 of the transpose of the state-transition matrix of the edge oscillation [17,18].

By evaluating $\Delta\Gamma$ for different input voltages and all of the perturbing cells, we obtain Fig. 7(b) by setting ω_1 to 2ω. At present, we are only required to elucidate the relative intensity of $\Delta\Gamma$, so we have omitted the legend for clarity. The brighter region indicates the greater $\Delta\Gamma$. The spatial dependence of $\Delta\Gamma$ is significant. Consistent with the behavior of the turnaround distance of the edge oscillation, cells exhibiting a greater $\Delta\Gamma$ become distant from the input as the input voltage A increases. The magnitude of $\Delta\Gamma$ depends mainly on A. As the input dc voltage increases, regions exhibiting greater and lesser $\Delta\Gamma$ appear alternately. Moreover, there are two peaks with the magnitude of $\Delta\Gamma$ at different input voltages. For example, points M_1 and M_2 correspond to two such peaks for $A = 0.45$ V. As mentioned above, the temporal waveform monitored at a fixed cell is a train of square pulses. Moreover, its duty cycle depends on the monitoring cell, which is a unique cell that exhibits a 50% duty cycle. Then there are two spectrally equivalent cells, for which the ratio of the "on-time" duration to the total period observed at one of the two cells is equal to that of the "off-time" duration to the total period observed at the other, both in front of and behind that cell. The two-peak property of the magnitude of $\Delta\Gamma$ is because the oscillating edge correlates most with the external perturbation at two spectrally equivalent cells.

IV. EXPERIMENTS

The test TD line was built on a standard breadboard. The shunt electronic switches were NEC 1S1763 Esaki diodes. Series inductance, resistance, and shunt capacitance were implemented using 1.0-μH inductors (TDK SP0508), 1.0-Ω resistors (Tyco Electronics CFR25J), and 470-pF capacitors (TDK FK18C0G1), respectively. First, we evaluated the spectral properties of the test line by connecting the input end to a dc voltage source and monitoring the voltage at the fifth cell using a spectrum analyzer (NEC Specat).[2] The result is shown in Fig. 8. In the region $A \leqslant 0.5$ V or 0.55 V $\leqslant A \leqslant 0.60$ V, the spectral peaks are effectively simulated by the calculated ones shown in Fig. 7(a). Therefore, the edge oscillation may be supported by the f mode in those regions. For other input dc voltages, the frequency corresponding to the lowest frequency peak is approximately twice as high as those expected in Fig. 7(a). Therefore, the edge oscillation can be supported by the s mode. Two mutually synchronized edges contribute to this oscillation mode. The turnaround distance of each edge

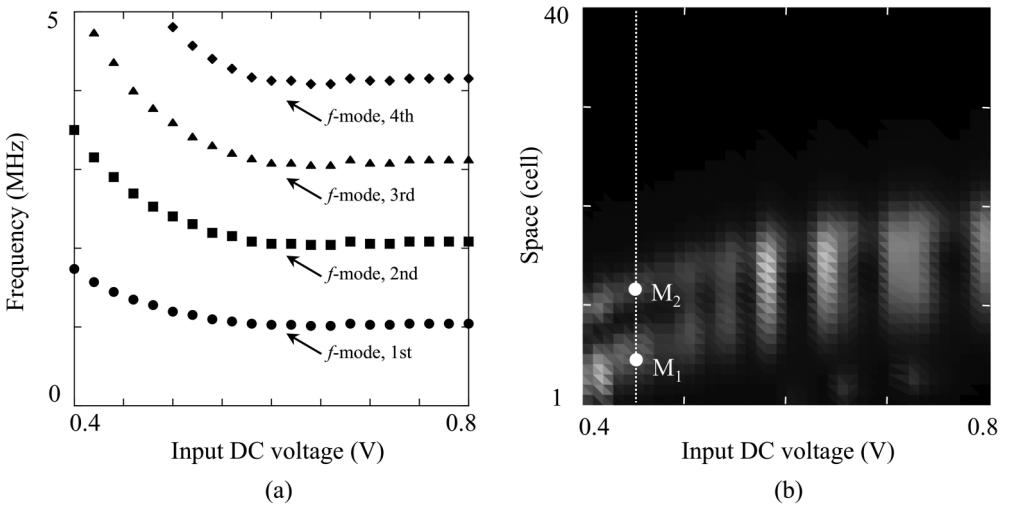

FIG. 7. Calculated properties of the test TD line. (a) Spectral peaks as a function of input dc voltage and (b) dependence of the phase sensitivity on space and input dc voltage. The spectral peaks are obtained by the Fourier transform of temporal waveforms monitored at the fifth cell. The dotted vertical line in (b) represents a slice at 0.45 V. Points M_1 and M_2 specify the peak positions for 0.45 V.

is approximately half of that of the single edge in the f mode; therefore, the frequency of the s mode becomes twice as high as that of the f one. Refer to Figs. 13 and 14 and their captions for a detailed description. The s mode in Fig. 7(a) cannot be accurately simulated by numerical calculations; this discrepancy may be because the calculation time is insufficient to identify the oscillation mode to which the line finally settles. Moreover, performance uniformity and noises in employed devices may influence the mode to which the edge oscillation should settle.

In order to examine the transient oscillation modes, we applied a square-pulsed voltage instead of dc to the input end. Figure 8(b) shows the result for a pulsed voltage having a duration of 266 μs. There are no clear spectral peaks at amplitudes lower than 0.5 V. The f mode may not establish sufficiently steady edge oscillations to exhibit high-quality factors at the spectral peaks. On the other hand, the f mode, which cannot be detected while inputting a dc voltage, coexists with the s mode at amplitudes higher than 0.5 V. The f mode may dominate the edge oscillation initially after excitation, and the s mode may then gradually substitute the f mode as time progresses.

Figure 9 shows the mode that dominates the edge oscillation for different pulse durations. The spectral intensities are obtained by the Fourier transform of the temporal waveform monitored at the fifth cell. Because of their small separation in frequency, the correlation between the fundamental component of the s mode and the second-harmonic component of the f mode must determine the mode that should dominate the edge oscillation. Squares and circles represent the spectral intensities at the fundamental frequency of the s mode and the second-harmonic frequency of the f mode, respectively, for an input amplitude of 0.7 V. The horizontal axis measures the pulse frequency, which is 0.8 times the inverse of the pulse

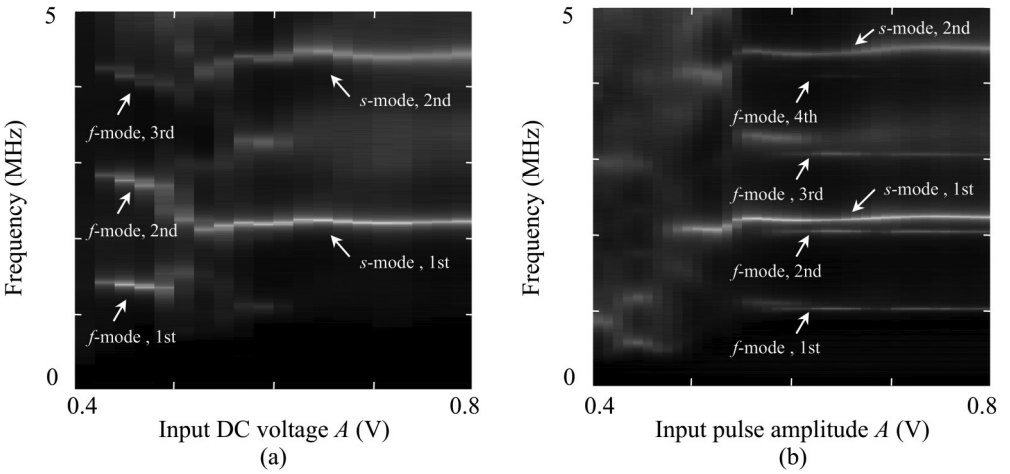

FIG. 8. Dominant oscillation modes in TD lines. Spectral intensities are plotted for several input voltages. (a) Spectrum measured with dc inputs and (b) spectrum measured with pulsed inputs. Spectral intensities were obtained by the Fourier transform of temporal waveforms monitored at the fifth cell. We identify which mode dominates the spectral peaks by the fundamental frequencies.

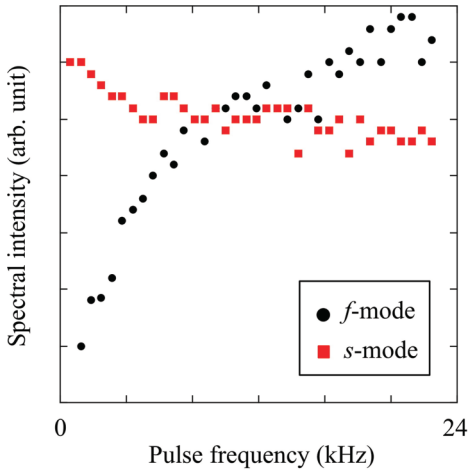

FIG. 9. (Color online) Dependence of peak intensities on pulse frequency. Circles: the spectral intensities at the second-peak frequency of the f-mode, squares: those at the first-peak frequency of the s-modes. The horizontal axis measures the pulse frequency defined by 0.8 times the inverse of the pulse duration.

duration. (The duty cycle was set to 80%.) We can observe that the s mode dominantly supports the edge oscillation for large pulse durations that correspond to a pulse frequency of <4 kHz. On the other hand, for pulse frequencies higher than 10 kHz, the f-mode intensity becomes greater than that of the s mode. These observations reinforce our expectation mentioned above.

In order to examine the external synchronization properties, we measured the locking range of frequency for sinusoidal perturbation. Two input voltages at which f-mode oscillation was observed for a dc voltage input were selected. A single cell was perturbed by a sinusoidal voltage. The frequency of sinusoidal perturbation was swept around the second-harmonic frequency of the f-mode oscillation to ensure consistency with the procedure used to obtain Fig. 7(b). The locking range was obtained by measuring the range of perturbation frequency at which the second-harmonic frequencies of the f-mode oscillation were in synchronization with the external frequency. By changing the perturbed cell, we obtained the spatial dependence of the locking range. The results are shown in Fig. 10(a). In Fig. 10(a), we observe that external synchronization is more efficient at 0.45 V than at 0.55 V. Moreover, the locking range becomes maximum at the 10th–11th and the 18th–19th cells for 0.45- and 0.55-V inputs, respectively. The highly efficient cells shift toward the far end as the input amplitude increases. The efficiency of external synchronization is significantly degraded near the sixth cell for a 0.45-V input, thereby resulting in the presence of two peaks. Qualitatively, the locking range of frequency must be effectively predicted by $\Delta\Gamma$. To examine the similarity, we show two vertical views in Fig. 7(b) for A values of 0.40 and 0.56 V. The two-peak property is clearly observed at $A = 0.40$ V, together with the spatial shift of the cell position by A. These properties effectively simulate the measured ones.

To detect the spatiotemporal behavior of the edge oscillation, we attempted to synchronize it with sinusoidal perturbation having a sufficiently low phase noise to measure the behavior. The line edge was excited by a 0.7-V square voltage with a duration of 266 μs. The perturbing signal was generated by an arbitrary waveform generator NF WF1974 and it was injected at the 17th cell, where $\Delta\Gamma$ was supposed to be maximum. The line voltages along the test TD line were detected by an Agilent 1134 active probe, and they were monitored in the time domain using an Agilent DSO90254A oscilloscope.

First, we established external synchronization by setting the frequency of perturbation to 2.05 MHz, which corresponded to the second-harmonic frequency of the f mode. The measured spatiotemporal voltages are shown in Fig. 11, and the brighter points correspond to higher voltages. The f-mode edge oscillation was successfully observed. Moreover, the calculated results shown in Fig. 5 are in good agreement with the measured ones. The forward and backward voltage edges are designated f and b, respectively. The voltage edge

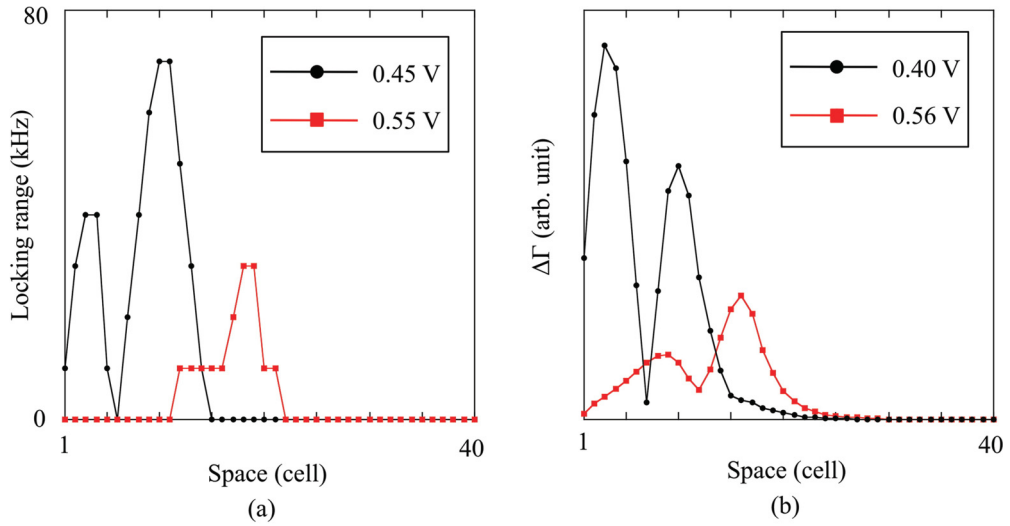

FIG. 10. (Color online) Efficiency of external synchronization. Spatial dependence of (a) the measure frequency locking range and (b) the numerically obtained $\Delta\Gamma$.

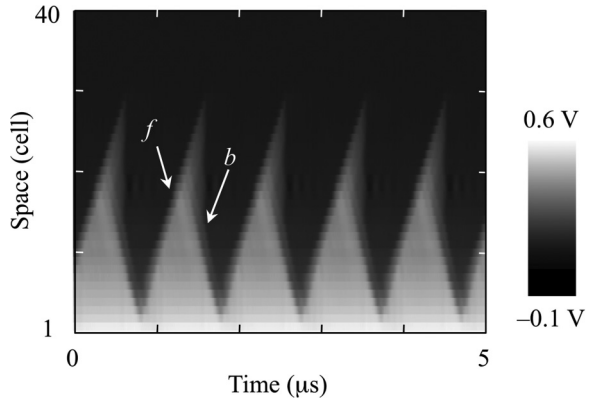

FIG. 11. Spatiotemporal behaviors of measured f-mode waveforms. The brighter points exhibit higher line voltages. The perturbation was applied at the 17th cell. Forward- and backward-going edges are designated f and b, respectively.

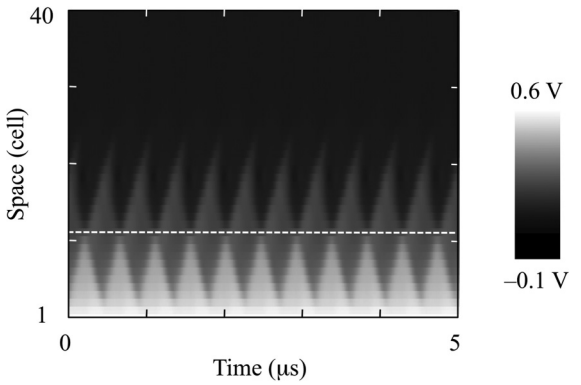

FIG. 13. Spatiotemporal behavior of the measured s-mode oscillating edge. Brighter points exhibit higher line voltages. The perturbation was applied at the 17th cell. The location of point P, where two voltage edges originate, is shown by the horizontal dashed line.

propagated from the input end to the 20th cell, and then it returned to the input end; the turnaround time was estimated to be 1.0 μs. As mentioned above, the forward edge was carried by an oscillatory mode whose speed is supposed to be lower than c_0 in Eq. (8). In addition, this slow propagation was predicted heuristically by the property of a TD line in which the short-wavelength waves propagated more slowly than the long-wavelength ones because of dispersion [11]. We observed that the forward edge was much slower than the backward one by monitoring five temporal waveforms at the cells numbered $n = 10$, 11, 12, 13, and 14, as shown in Fig. 12. The rising and falling pulse transients result from the forward- and backward-moving voltage edges (the rising transient progresses from $n = 10$ to $n = 14$, whereas the falling transient progresses in the reverse direction). Therefore, we can obtain their speed by estimating the elapsed time that is required to pass through the cells ($\Delta t_{f,b}$ in Fig. 12). We observed that $\Delta t_f > \Delta t_b$. The actual speeds of the forward and backward edges were estimated to be 2.5×10^7 and 4.2×10^7 cells/s, respectively.

Second, another external synchronization was established by setting the frequency of perturbation to 2.21 MHz, which corresponds to the fundamental frequency of the s mode. Figure 13 shows the measured spatiotemporal voltages, and the s mode was successfully detected. Two mutually synchronized voltage edges, each of which originates at a fixed point, are shown by the horizontal dashed line in Fig. 13. The turnaround time is estimated to be 0.45 μs, which is half that of the f mode. In Fig. 13, we observe that the turning point of a single edge is near the 20th cell.

Figure 14 illustrates the s-mode edge oscillation. For the s mode, the voltage steadily oscillates across V_p at a fixed point on the line, which is shown as P in Fig. 14. Then a voltage edge may originate at P and propagate forward at the time at which the voltage at P becomes higher than V_p. In contrast, when the voltage at P becomes lower than V_P, a voltage edge can originate at P and start propagating backward. Each edge oscillation is a limit cycle and can establish mutual synchronization with the other; therefore, the two voltage

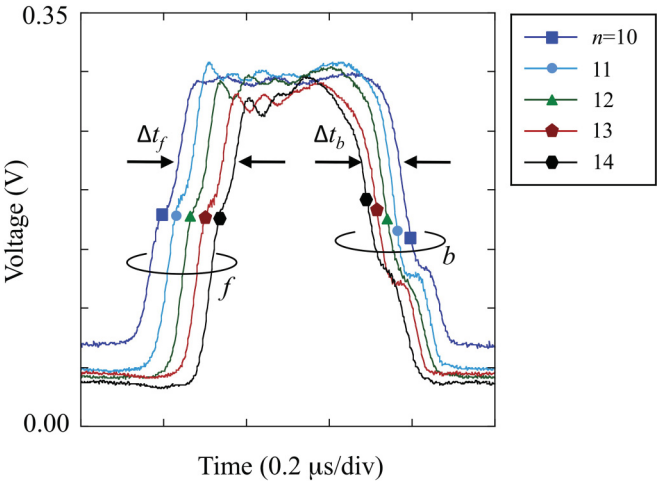

FIG. 12. (Color online) Temporal waveforms monitored at fixed cells. Five waveforms, monitored at $n = 10$, 11, 12, 13, and 14, are shown for a 1-μs duration, where n is the cell number. Rising and falling pulse transients, bundled with f and b, result from the passing forward and backward voltage edges.

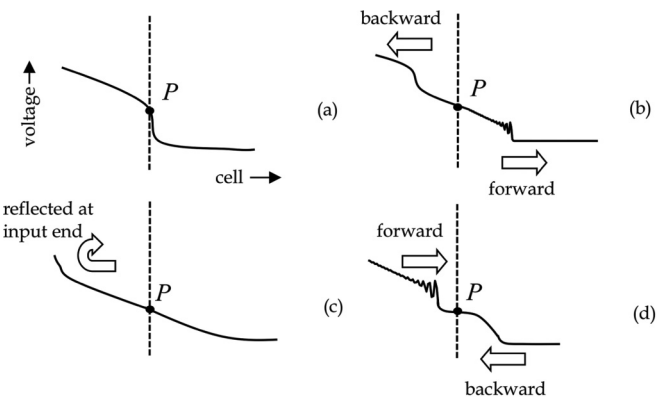

FIG. 14. Secondary oscillation mode of the pulse edge in a TD line. Time progresses from (a) to (d). The approaching edges in (d) arrive at point P again as in (a), resulting in edge oscillation. The horizontal axis measures the spatial dimension, which must be originally discrete.

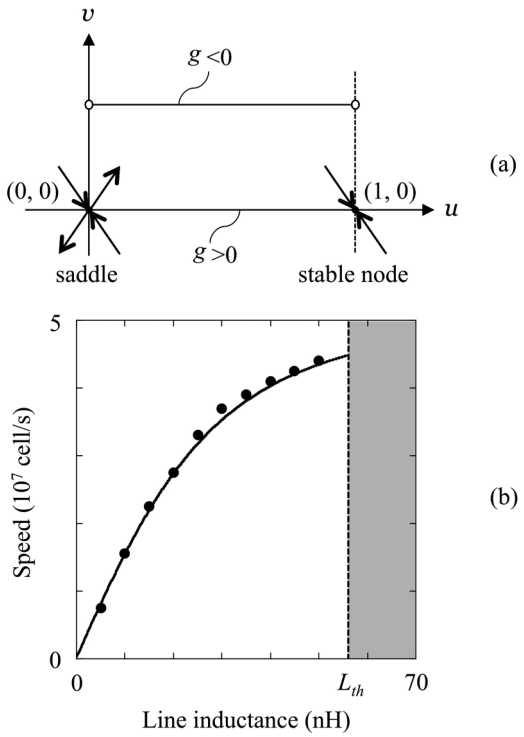

FIG. 15. Traveling fronts in TD lines for $c \in (c_0, 1/\sqrt{LC})$. (a) Critical points in the phase plane for $c \in (c_0, 1/\sqrt{LC})$ and (b) dependence of the speed of the traveling front on the line inductance. The curve in (b) represents the minimum speed c_0 defined by Eq. (8). Circles show the numerically estimated speeds. $L_{\rm th}$ is defined by $CR/|G_1|$.

edges are eventually phase locked. Figure 14 illustrates this process. For clarity, the line voltage at P is shown to be time invariant. Two oscillating edges originate at P in Fig. 14(a). One of the two edges starts propagating backward toward the input end, and the other propagates forward, as in Fig. 14(b). The backward voltage edge reaches the input end and is reflected. Almost simultaneously, the forward voltage edge turns to propagate backward [Fig. 14(c)]. Then both the edges propagate to point P [Fig. 14(d)] and recover their initial states shown in Fig. 14(a). Because the s mode results from a mutual synchronization, its phase noise may become smaller than that of the f mode [12]. Because of the reduced turnaround time, the oscillation frequency of the s mode becomes higher than that of the f mode for a given input dc voltage. Moreover, to establish a mutual synchronization between the two edges, oscillation frequencies must be approximately equal to each other; therefore, the s mode exhibits an oscillation frequency that is approximately twice as high as that of the f mode.

V. CONCLUSION

The external synchronization of the oscillating edge(s) on a TD line was investigated using numerical and experimental methods. The predictions made by the phase-evolution equation were validated by the experimental observations. Moreover, we successfully detected the spatiotemporal behaviors of oscillating edges carried by both the f and the s modes. The edge oscillation has noteworthy properties such as the voltage-controlled oscillation frequency and spatial extendedness. This study lays the foundation for the description of more complex behaviors of edge oscillations on TD lines.

APPENDIX: PROPERTIES OF TRAVELING FRONTS AND SHOCK WAVES

In this Appendix, the condition required to develop either a traveling front or a shock wave is derived together with several results of numerical calculations that validate the analytical ones.

When $CR + LdI_D/dV > 0$ for all $u \in (0,1)$, the system satisfies all of the assumptions required in Theorem 1 of [14] for $c \in (c_0, 1/\sqrt{LC})$; therefore, it has been shown that a unique traveling front is supported by a TD line. Figure 15(a) shows the corresponding phase portrait. Because I_D is finite in $u \in (0,1)$, we can construct a line $v = \bar{v}$, where $g < 0$. Moreover, g becomes positive on the u axis [$g(u,0,c) = RI_D(V_{\rm th}u)/V_{\rm th}(1 - c^2LC) > 0$]. Then there must be a trajectory starting from P_1 at $\xi = -\infty$ and reaching P_2 at $\xi = +\infty$, which corresponds to a front transition from $V = V_{\rm th}$ to 0.0 (t becomes $\mp\infty$ at $\xi = \pm\infty$). Figure 15(b) shows the calculated speed of the front for different values of L, with $1/\sqrt{CL}$ being kept fixed at 4.5×10^{-7} cell/s. I_D was tuned such that the maximum current in (0, $V_{\rm th}$) becomes 1.0 mA. Moreover, R, $V_{\rm th}$, and V_0 were set to 0.4 Ω, 0.5 V, and 1.0 V,

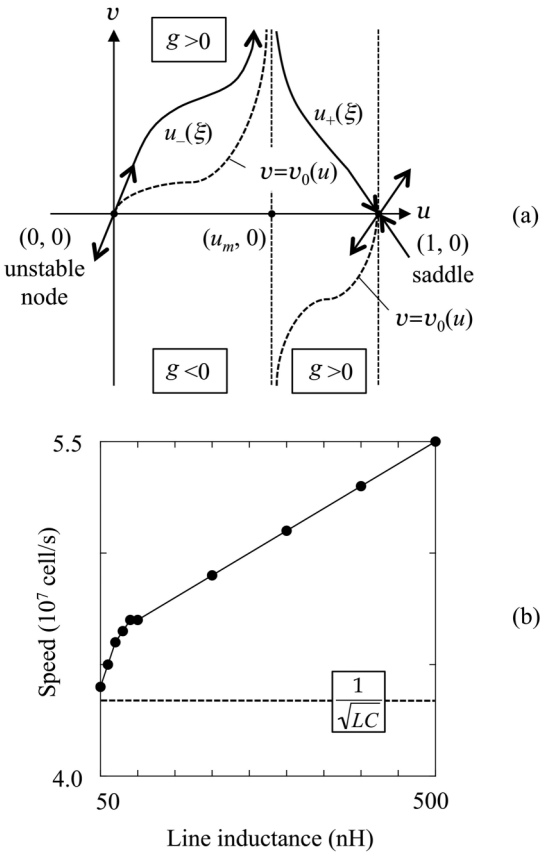

FIG. 16. Traveling fronts in TD lines for $c > 1/\sqrt{LC}$. (a) Critical points in the phase plane for $c > 1/\sqrt{LC}$ and (b) dependence of the speed of the traveling front on the line inductance. Circles show the numerically estimated speeds in (b).

respectively. The curve and circles represent the minimal speed c_0 defined by Eq. (8) and the numerically estimated speeds, respectively. The uppermost inductance $L_{\rm th}$ satisfies $CR + L_{\rm th}G_1 = 0$, where $c_0 = 1/\sqrt{CL}$. Interestingly, each numerically obtained front exhibits the lowest realizable speeds.

For larger c, there is no trajectory that directly connects P_1 and P_2. However, when the line permits a single solution for $u = u_m \in (0,1)$ for $CR + LdI_D(V_{\rm th}u)/dV = 0$, two trajectories $u_\pm(\xi)$ can be present, and we can construct a trajectory $u_s(\xi)$, such that $u_s = u_-$ for $u \in (0,u_m)$ and $u_s = u_+$ for $u \in (u_m,1)$. Figure 16(a) shows the trajectories in the phase plane. The phase plane is divided into three parts by the function $v = v_0(u)$, which is defined by

$$v_0(u) = \frac{RI_D(V_{\rm th}u)/V_{\rm th}}{c\,(CR + LdI_D(V_{\rm th}u)/dV)}, \tag{A1}$$

where g vanishes. On the basis of the assumption, v_0 becomes $\pm\infty$ for $u = u_m \mp 0$. The region in the phase plane sandwiched by the two branches of v_0 exhibits $g < 0$, whereas g becomes positive for the remaining regions except for v_0. For $c > 1/\sqrt{LC}$, P_1 and P_2 are an unstable node and a saddle, respectively. The solid curves show $u_\pm$. It is easily seen that both the main and the side directions of P_1 are contained in the region $g > 0$. Moreover, the stable direction of P_2 is contained in the region $g < 0$. Because $u'_\pm$ increases near u_m, u_s describes a shock wave. Figure 16(b) shows the calculated speed for line inductances that are larger than those used to obtain Fig. 15(b). For these inductances, we observed a voltage edge with a very steep transient, whose speed was greater than $1/\sqrt{LC}$ and depended linearly on the line inductance.

[1] A. Scott, *Neuroscience: A Mathematical Primer* (Springer, Berlin, 2002).

[2] J. Nagumo, S. Arimoto, and S. Yoshizawa, Proc. IRE **50**, 2061 (1962).

[3] I. Richer, IEEE Trans. Circuit Theory **13**(4), 388 (1966).

[4] A. Scott, *Active and Nonlinear Wave Propagation in Electronics* (Wiley-Interscience, New York, 1970).

[5] M. Asada, S. Suzuki, and N. Kishimoto, Jpn. J. Appl. Phys. **47**, 4375 (2008).

[6] E. Ruai, Y. Yu, Y. Konishi, S. T. Allen, M. Reddy, and M. J. W. Rodwell, IEEE Microwave Guided Wave Lett. **4**, 220 (1994).

[7] G. Bartolucci, M. Dragoman, R. Marcelli, and F. Pini, Int. J. Infrared Millimeter Waves **16**, 1719 (1995).

[8] M. J. W. Rodwell, S. T. Allen, R. Y. Yu, M. G. Case, U. Bhattacharya, M. Reddy, E. Carman, M. Kamegawa, Y. Konishi, J. Pusl, and R. Pullela, Proc. IEEE **82**, 1037 (1994).

[9] K. Narahara and A. Yokota, IEICE Electron. Express **5**, 973 (2008).

[10] B. Z. Essimbi and D. Jäger, J. Infrared Milli. Terahz. Waves **33**, 627 (2012).

[11] K. Narahara, J. Appl. Phys. **100**, 064908 (2006).

[12] A. Pikovsky, M. Rosenblum, and J. Kurths, *Synchronization: A Universal Concept in Nonlinear Sciences* (Cambridge University Press, New York, 2001).

[13] Y. Kuramoto, *Chemical Oscillations, Waves, and Turbulence* (Springer-Verlag, New York, 1984).

[14] K. P. Hadeler, Proc. Edinburgh Soc. **31**, 89 (1988).

[15] K. P. Hadeler and F. Rothe, J. Math. Bio. **2**, 251 (1975).

[16] A. Yokota and K. Narahara, Jpn. J. Appl. Phys. **48**, 084502 (2009).

[17] E. M. Izhikevich, SIAM J. Appl. Math. **60**, 1789 (2000).

[18] F. Hoppensteadt and E. Izhikevich, *Weakly Connected Neural Networks* (Springer-Verlag, New York, 1997).